Carbohydrate Polymer Technologies and Applications 3 (2022) 100219

Contents lists available at ScienceDirect

Carbohydrate Polymer Technologies and Applications

journal homepage: www.sciencedirect.com/journal/carbohydrate-polymer-technologies-and-applications

Nitro-oxidation process for fabrication of efficient bioadsorbent from lignocellulosic biomass by combined liquid-gas phase treatment

Hui Chen [a], Kai Chi [a], Rangjian Cao [a], Sunil K. Sharma [a], Syed M.Q. Bokhari [b], Ken I. Johnson [a], Duning Li [a], Priyanka R. Sharma [a], Benjamin S. Hsiao [a,*]

[a] Department of Chemistry, Stony Brook University, Stony Brook, New York 11794-3400, United States
[b] Department of Agricultural and Biological Engineering, The Pennsylvania State University, University Park, PA 16802, United States

ARTICLE INFO

Keywords:
Biomass
Delignification
Cellulose oxidization
Nitric acid
Nitrogen dioxide
Bioadsorbent

ABSTRACT

A sequential treatment involving HNO_3 delignification in liquid phase and NO_2-induced cellulose oxidation in gas phase was applied to raw jute fibers. The structure, chemical compositions, morphology and surface properties of the treated materials in each step were systematically characterized. First, delignification of jute fibers could occur at a mild HNO_3 condition (30%, 25 °C, 6 h), capable of removing a significant portion of lignin without changing the native cellulose I structure. Subsequently, gas-phase NO_2 treatment can oxidize partially delignified jute fibers and produce high concentrations of carboxyl groups (1.31–1.45 mmol/g) on the material surface, comparable to TEMPO-mediated oxidation. The resultant material is effective in removing positively charged contaminants, such as Thallium(I) ions from water (the removal efficiency >80%). The mixed liquid-gas phase nitro-oxidation process (NOP) provides better control of cellulose oxidation for fabrication of water remediation adsorbents from lignocellulose biomass and further reduces the energy and water consumption since there is no requirement for washing the oxidized cellulose after gas-phase NO_2 treatment.

1. Introduction

The demand for sustainable energy sources from industry, consumers and government (Moon et al., 2011; Klemm et al., 2005; Ball, 2005) is increasing continuously since petroleum-based fuels are unstainable in nature. (Agarwal, 2007) Furthermore, the emerging crisis related to climate changes due to the rapid increase in greenhouse gas emissions and urbanization and has prompted us to look for new solutions to enhance the resilience and sustainability of the food, energy and water nexus systems (Fatma et al., 2018, Lin et al., 2014). The present study represents one of our attempts to demonstrate a solution that can upcycle diverse lignocellulosic biomass sources, especially from underutilized biomass feedstocks, into efficient water remediation materials. These biomass sources include both woody and non-woody plants, where the latter is relatively underutilized. The major application of non-woody plants, such as agriculture residues, is the production of biofuel (Li et al., 2017). For example, biofuels are currently produced from 1.3 billion tons of lignocellulosic residues, mostly from agricultural residues, such as wheat, corn, soybean, and sugarcane in the United States (Perlack et al., 2005). It is thought that these biomass sources can replace up to 40% of the fuel consumption, however, the high water consumption to grow energy crops has also cast doubt with the long term sustainability of such apprach (Perlack et al., 2005, Zheng et al., 2007). In this study, we demonstrate that these non-woody biomass sources are also good feedstocks to extract efficient remediation materials for water purification.

Lignocellulosic biomass consists of three major components: cellulose (40–60%), hemicellulose (20–40%), and lignin (10–24%) (Sharma et al., 2019; Putro et al., 2016), where the compositions of these components vary from different sources . Cellulose, as the most important skeletal component, is a nature polymer consisting of β-1,4 linked D-glucose subunits that are aggregated by hydrogen-bonding and van der Waals forces. With the repeated unit of D-glucose, cellulose can be easily functionalized due to the abundant hydroxyl groups and can be used in varying applications after modifications (Sharma et al., 2020). Cellulose in biomass appears in both crystalline and amorphous forms. The amorphous cellulose region can be easily hydrolyzed, whereas modification or defibrillation of the crystalline cellulose region requires chemical treatments, such as dilute acids, alkalis and cellulolytic enzymes due to the strong interchain interactions (hydrogen-bonding and

* Corresponding author.
E-mail addresses: priyanka.r.sharma@stonybrook.edu (P.R. Sharma), benjamin.hsiao@stonybrook.edu (B.S. Hsiao).

https://doi.org/10.1016/j.carpta.2022.100219

Available online 18 May 2022

van der Waals forces) (Kumar et al., 2009; Rabelo et al., 2014). Hemicellulose is a polysaccharide mixture, composed of pentose (C5) and hexose (C6) sugars, such as glucose, mannose, xylose, and arabinose along with sugar-acids (e.g., methylglucuronic acid and galacturonic acid). Lignin is a phenyl propane polymer linked with ester bonds that tightly binds cellulose and hemicellulose together, forming a complex network (Kumar et al., 2009). In general, non-woody biomass feedstocks, such as agriculture residues and grasses, have lower lignin contents than those from woody plants, such as softwoods and hardwoods (Cosgrove & Jarvis, 2012; Bernal-Lugo et al., 2019)

In biofuel production, the pretreatment of biomass feedstocks to remove the lignin component, reduce cellulose crystallinity and increase the surface area, is an essential but costly first step (Wyman et al., 2005). The typical pretreatment processes can be categorized into five types: physical (Galbe & Zacchi, 2007; Cadoche & López, 1989), chemical (Esteghlalian et al., 1997; Kim & Holtzapple, 2006; Bjerre et al., 1996), electrical (Ho & Mittal, 1996; Angersbach et al., 2000; Kumar et al., 2011), biological (Wichern et al., 2004; Itoh et al., 2003), and a combination of these. Among these methods, chemical pretreatments such as sulfite and alkaline pulping (delignification) processes that have been adopted by the papermaking industry are most common (Bajpai, 2018; Wool, 2005). These pretreatment processes are mainly developed to process woody plants and can offer different advantages depending on the feedstock materials. For example, technologies such as solvent-based or organosolv pulping processes are in general more selective for hardwoods than softwoods (Jiménez et al., 1997; McDonough, 1992) However, the general drawback of the above pretreatment processes are the need for large chemicals consumption (Wool, 2005), low selectivity in reaction (McDonough, 1992) and long processing time (Jiménez et al., 1997). It is clear that a simpler, more cost-effective and environmentally friendly pretreatment process can be developed for the delignification process of non-woody biomass feedstocks.

In our lab, we have developed a simple nitro-oxidation process (NOP) to extract cellulose nanofiber (CNF) from a variety of biomass feedstocks (Chen et al., 2021; Sharma et al., 2018, 2017). In NOP, only two chemicals: nitric acid (HNO_3) and sodium nitrite ($NaNO_2$), are involved, both are ingredients that can be used to synthesize fertilizers. NOP combines the steps of pulping and cellulose oxidation. Nitric acid pulping has a long history dating back to the 19th century. The presence of nitrogen oxide species can depolymerize the lignin component by converting the syringyl units in lignin into soluble benzoquinone products, whereas the hemicellulose component can be broken down by nitric acid into xylose and other byproducts, both soluble in water. In spite of extensive efforts (Rydholm, 1965; Bolker, 1965; Cox & Worster, 1971; Engstrom & Samuelson, 1984), this technology has never become a successful pulping technology. There are several reasons for this, including the high cost of nitric acid (unless produced on-site), non-uniform pulping from wood chips, the need of good impregnation of starting wood chips, and deteriorated pulp strength properties due to cellulose hydrolysis and toxicity problems from nitrogen oxides.

The mechanism of oxidation of cellulose at the C6 position using this method is as follows (Chen et al., 2021). HNO_2 is formed by the reaction of $NaNO_2$ and nitric acid (HNO_3). Subsequently, HNO_2 liberates nitroxonium ions (NO^+) in the presence of excess acid. The produced NO^+ can attack the primary hydroxyl group of cellulose at the C6 position and produce aldehyde group via nitrite ester (R-CH_2-O-NO), which is an intermediate and subsequently decomposes in acidic medium to generate HNO and aldehyde group at the C6 position on cellulose. The excess nitric acid oxidizes HNO to HNO_2 and the oxidation cycle continues. Thus, nitric acid is consumed as the reaction proceeds and HNO undergoes self-dissociation to N_2O (nitrous oxide) and water molecule (Strojny et al., 1971). The produced aldehyde group on cellulose, then oxidizes into carboxyl group in the presence of hydronium ion. The NOP approach effectively reduced the need for multiple chemicals and offered more than 60% energy savings when compared to conventional multi-step processes in converting raw biomass into CNFs. In addition, the effluent from this method could be efficaciously neutralized using base (e.g., sodium hydroxide and potassium hydroxide) to produce nitrogen rich salts as plant fertilizers. The idea of using the spent liquor as a fertilizer was first demonstrated by Brink and coworkers (Brink, 1961; Brink et al., 1961). Hence, NOP is a promising and sustainable route to prepare carboxyl-CNF in a more cost-effective way. The obtained CNF with sufficient carboxyl groups can be applied in water purification. For example: CNF can act as an adsorbent and flocculant to remove the toxic metal ions and dyes impurities (Chen et al., 2021; Sharma et al., 2018, 2017; Chen et al., 2019; Sharma et al., 2018).

We noted that the demonstrated NOP as a one-pot approach using concentrated HNO_3 ($> 60\%$) encountered several technical challenges for large scale operation that need to be overcome. These challenges included: handling of concentrated nitric acid (60%), disposal of a large amount of reaction effluent after neutralization, difficult control of cellulose oxidation (e.g., due to possible thermal runaway), and multiple-purification steps to obtained nanocellulose. The present study represents our efforts to improve the demonstrated NOP thus far, using raw jute fibers as a model system. As the one-pot reaction NOP (in the liquid state) is difficult to control the pulping and cellulose oxidation processes precisely, we have designed a sequential process that involves the HNO_3 pulping first in the liquid state and the cellulose oxidation using NO_2 (an effective cellulose oxidizing agent) (Cox & Worster, 1971; Engstrom & Samuelson, 1984; Strojny et al., 1971; Brink, 1961) in the gaseous phase next. In addition, we have systematically reduced the HNO_3 concentration as we hypothesize that low concentrations of can HNO_3 effectively remove most of the hemicellulose and lignin components in non-woody plant (i.e., jute) with a lower lignin content of and a porous cell wall structure. Furthermore, we modify this liquid-gas mixed phase NOP approach to only convert (or activate) raw biomass into bioadsorbents (thru partial defibrillation) with adsorption ability similar to activated biochar (or activated carbon). The structure, chemical compositions, morphology and surface properties of the treated jute materials in each step were systematically characterized.

2. Experimental

2.1. Materials

Raw (untreated) jute fibers (with degree of polymerization, DP ~ 520) were provided by Toptrans Bangladesh Ltd. in Bangladesh; Analytical grade nitric acid (ACS reagent, 65%) and sodium nitrite (ACS reagent ≥97%) were purchased from Sigma-Aldrich. Thallium(I) acetate (≥ 99%) was purchased from Sigma-Aldrich. All chemicals were used without further purification. Deionized (DI) water was produced in our lab.

2.2. NOP treatments of raw jute fibers

Different NOP treatments were employed to study the sequential delignification and oxidation steps of raw jute fibers. Firstly, the pulping step was carrying out using different HNO_3 acid concentrations and reaction temperatures. Subsequently, the HNO_3 treated jute fibers were oxidized in two different approaches for comparison: (i) by gas-phase (NO_2) treatment; (ii) by liquid-phase (HNO_3-$NaNO_2$) treatment. The detailed preparation conditions and codes used for the treated samples are summarized in Table 1. In brief, the notation NP represents the samples pretreated with HNO_3, GO represents the NO_2 (gas phase) oxidized samples, while LO denotes HNO_3-$NaNO_2$ (liquid phase) oxidized samples. These terms are followed by some digits that represent the treatment conditions (temperature-HNO_3 concentration in %).

2.2.1. HNO_3 pulping of raw jute fibers

Raw jute fibers were ground into a fine powder form with a particle size of 1 mm before used. In a typical pulping treatment, 10 g of ground jute fibers was loaded into a 3 L round bottom flask for HNO_3 treatment.

Table 1
Summary on the preparation of different samples and their codes (NP represents the HNO_3 treated sample, LO stands for the liquid-phase (HNO_3-$NaNO_2$) oxidized sample, GO denotes the gas-phase (NO_2) oxidized sample, and the numbers after each letter imply the treatment conditions (temperature-HNO_3 concentration in %).

Sample Code	Reaction Conditions
NP25-15	15% HNO_3 treatment at 25 °C
NP25-30	30% HNO_3 treatment at 25 °C
NP25-40	40% HNO_3 treatment at 25 °C
NP25-50	50% HNO_3 treatment at 25 °C
NP25-60	60% HNO_3 treatment at 25 °C
NP40-15	15% HNO_3 treatment at 40 °C
NP40-30	30% HNO_3 treatment at 40 °C
NP40-40	40% HNO_3 treatment at 40 °C
NP40-50	50% HNO_3 treatment at 40 °C
NP40-60	60% HNO_3 treatment at 40 °C
GO1	(i) HNO_3 treatment: 25 °C at 30% (ii) Gas-phase treatment: 30 mole% NO_2 gas at 43°C
GO2	(i) HNO_3 treatment: 40 °C 30% (ii) Gas-phase treatment: 3-10 mole% NO_2 gas at 24°C
LO1	(i) HNO_3 treatment: 25 °C at 30% (ii) Liquid-phase treatment: 30% HNO_3+ 0.14 mol $NaNO_2$
LO2	(i) HNO_3 treatment: 25 °C at 30% (ii) Liquid-phase treatment: 60% HNO_3+ 0.14 mol $NaNO_2$
LO3	(i) HNO_3 treatment: 40 °C at 30% (ii) Liquid-phase treatment: 30% HNO_3+ 0.14 mol $NaNO_2$
LO4	(i) HNO_3 treatment: 40 °C at 30% (ii) Liquid-phase treatment: 60% HNO_3+ 0.14 mol $NaNO_2$

Then, 140 mL of HNO_3 (at varying concentration of 15, 30, 40, 50 and 60%) was added into the round bottom flask for 6 h of pretreatment under stirring in a sealed environment. The reaction temperature was set at 25 °C and 40 °C, respectively. After the pretreatment, samples were extracted and washed with deionized (DI) water until the conductivity of the supernatant was lower than 20 μS/cm. Afterward, the recovered products (delignified Jute Fibers) were oven-dried at 80 °C for 24 h for further study.

2.2.2. *Gas-phase oxidation (NO_2) of delignified jute fibers*

The experimental setup diagram of the gas-phase treatment is illustrated in Fig. 1. The applied reaction procedures were as follows. Firstly, humidified nitrogen (N_2 with 50 % relative humidity (RH)) was passed through the dry sample column for 1 h to introduce moisture. Then, two selected NO_2 and dry N_2 gas mixtures (composition is shown in Table 1) were used to purge into the sample column to induce oxidation reaction separately. The reactor outlet temperature and the outlet gas composition were monitored until the reactor outlet gas composition was stabilized. After that, the gas flow was stopped and the NO_2 gas was retained in the reactor for about 3 h. Subsequently, warm and humidified N_2 (40 °C, 50 % RH) was passed through the reactor to flush out NO_2 and the byproducts (e.g. cellulose nitrite). Finally, dry N_2 was passed through the reactor overnight to flush out residual NO_2 and remove HNO_3 residues. In this reaction, two HNO_3 treated samples (i.e., NP25-30 or NP40-30, 30 g each) were chosen for the gas-phase reaction (NO_2 gas concentration and temperature are summarized in Table 1. For sample GO1, 30 mole% NO_2 gas was used, and the temperature was set to 40 °C, while for sample GO2, 3-10 mole% NO_2 gas was used, and the temperature was set to 24 °C. After the gas-phase treatment, samples were washed by DI water to remove residual hemicellulose and then oven-dried for further characterization.

2.2.3. *Liquid-phase oxidation (HNO_3 and $NaNO_2$) of delignified jute fibers*

Liquid-phase oxidation was also applied to two HNO_3 treated samples (i.e., NP25-30 and NP40-30) using our previous liquid-phase NOP approach (Chen et al., 2021; Sharma et al., 2017). The specific reaction conditions for liquid-phase oxidation are shown in Table 1. Four treatment conditions were adopted as follows. For samples LO1 and LO3, 10 g of NP25-40/NP40-30 sample was placed in the 3-neck round bottom flask used, where 140 mL of 30% HNO_3 was gradually added to immerse all the fibers. Subsequently, 0.14 mol (9.6 g) of $NaNO_2$ was added to start the oxidation. For sample LO2 and LO4, 10 g of NP25-40/NP40-30 sample was treated with 60% of HNO_3 and 0.14 mol (9.6 g) of $NaNO_2$. All liquid-phase oxidation experiments were carried out under mild stirring for 12 h at room temperature. After the liquid-phase treatment, the resulting sample was washed by DI water until the pH level of the supernatant reached neutral. The final product was then oven-dried for characterization.

2.3. *Thallium(I) remediation test*

A series of simulated Thallium(I) solutions from 1 to 125 ppm were prepared by dissolving TI(I) acetate into DI water. The obtained GO1, GO2 and LO4 samples were used as adsorbents. In this study, a 2 mL of Tl (I) solution was remediated by 20 mg of GO and LO samples,

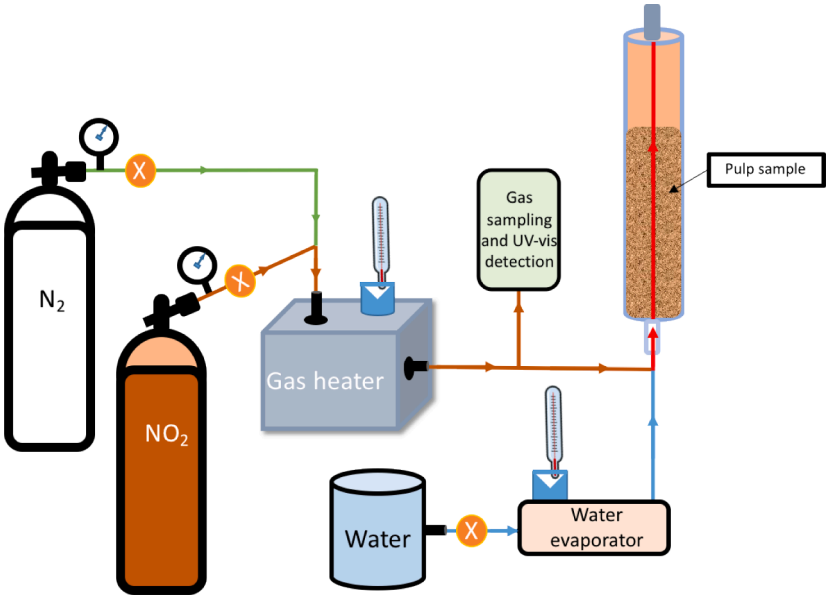

Figure 1. The schematic diagram of the gas phase experimental setup.

respectively. After 24 h of contact with the GO and LO samples, the treated aqueous solution was filtered out for the ICP-MS analysis. The filtrate was diluted by 10 times due to the detection limit of the ICP-MS instrument.

2.4. Characterization

The structures, chemical composition, morphology, and thermal properties of different HNO_3 treated samples were first characterized by Fourier Transform Infra-Red Spectrometry (FTIR) in the attenuated total reflectance (ATR) mode, High-performance Liquid Chromatography (HPLC), wide-angle X-ray diffraction (WAXD), solid state ^{13}C cross polarization-magic angle spinning nuclear magnetic resonance (^{13}C CP-MAS NMR), thermogravimetric analysis (TGA), and scanning electron microscopy (SEM). Both gas-phase and liquid-phase treated samples were subsequently characterized by FTIR, Brunauer-Emmett-Teller (BET) surface analysis and conductometric titration techniques. In the remediation test of GO and LO samples, Tl(I) concentration was measured by inductively coupled plasma mass spectroscopy (ICP-MS). Descriptions of the chosen characterization instruments and their experimental conditions used are summarized in the *Supporting Information*.

3. Results and discussion

3.1. HNO_3 pretreatment of jute fibers

The use of HNO_3 as a delignification (pulping) agent can yield pulp fiber with different characteristics, depending on the HNO_3 concentration and treatment temperature used. The results on the reaction yield, crystallinity index (CI) and crystal size (along different reflection plane) for varying HNO_3 treated samples are summarized in Table 2. It was observed that the yield of the products decreased with an increase in the HNO_3 concentration and pulping temperature. The decrease in yield implied the increase in degradation and removal of non-cellulosic components, such as lignin, hemicellulose, and other extractives. This is consistent with the process of acid hydrolysis (e.g., HNO_3) of non-cellulosic components, which generally produces water-soluble oligosaccharides, monosaccharides, and small chain aromatic polymers that can be removed by water washing. Based on the literature, raw jute fibers are comprised of the following compositions: cellulose (58-63%), hemicellulose (21–24%), lignin (12–14%) and extractive (< 3%) (Abdullah et al., 1978), where the yield results are generally consistent with these reported compositions.

Table 2
The results on yield, crystallinity index (CI) and crystal size (along different reflection plane) for varying HNO_3 treated samples.

HNO_3 treated samples	Yield (%)	CI (%) from WAXD	CI (%) from NMR	Cellulose I ($1\bar{1}0$) (nm)	Cellulose I (110) (nm)	Cellulose I (200) (nm)
NP25-15	75.18	59.76	50.9	2.80 ±0.05	3.63 ±0.05	3.83 ±0.05
NP25-30	61.47	61.56	51.2	3.20±0.1	3.90±0.1	3.96 ±0.03
NP25-40	50.45	66.41	51.6	3.35 ±0.15	3.97 ±0.21	4.03 ±0.05
NP25-50	47.83	71.49	56.9	3.37 ±0.06	4.20±0.1	4.17 ±0.03
NP25-60	45.53	63.34	54.7	3.77 ±0.03	5.73 ±0.17	3.60±0
NP40-15	66.12	62.96	49.7	3.00±0	3.47 ±0.03	3.76 ±0.03
NP40-30	50.34	68.93	49.8	3.30±0	3.40±0	4.00±0
NP40-40	46.48	72.63	55.8	3.53 ±0.16	5.30±0.1	4.20±0
NP40-50	42.08	69.32	60.2	2.70±0	5.53 ±0.05	4.26 ±0.03
NP40-60	30.54	59.24	59.0	2.97 ±0.13	5.43 ±0.23	4.40±0

The measured chemical composition of HNO_3 treated jute fibers are summarized in Fig. 2 (also Table S1 in *Supporting Information*). It was seen that the lignin content decreased from 15.85 with 15% HNO_3 treatment to 5.4% when 30% HNO_3 was used at 25°C. Based on the lignin composition of jute reported in the literature, we argued that the use of 15% HNO_3 probably did not remove the lignin component (if any, the degree of delignification was very small), where the use of 30% HNO_3 could effectively remove a large portion of lignin. In the NP25-60 sample (i.e., with 30% HNO_3), the lignin content became very low (2.35%), which indicate the successful delignification process. These results are similar to the literature, which is somewhat limited on the similar subject. For example, the treatment of wheat straw using the acetic acid-HNO_3 mixtures (i.e., 80% acetic acid and various higher concentrations of HNO_3) at high temperature (120°C) and long treatment time (10–20 h) also led to a significant decrease in the lignin content (the lowest final residual lignin content was 2.1%) (Sun et al., 2004). In another study, rice straw was treated with formic acid (90%) at 100°C, where 15.2% residual lignin was reported (Lam et al., 2001).

In Fig. 2, the hemicellulose content in the NP40-30 sample exhibited a significant drop (e.g. from 14.23% in the NP25-15 sample with little or no delignification) to 4.41%. This confirmed that the mild HNO_3 (30%) treatment was efficient to remove large portions of both lignin and hemicellulose components, although the treatment temperature needed to relatively high (i.e., 40°C). For example, in NP25-30, the lignin content was 5.40% and the hemicellulose content was 10.42%, where in NP40-30: the lignin content was 4.71% and the hemicellulose content was 4.41%. It was seen that the increase in HNO_3 concentration could enhance the removal of lignin and hemicellulose. However, with the highest concentration of HNO_3 (60%) used, the generation of excess extractives also became leger (e.g. 7.44% at 25°C and 9.88% at 40°C) indicating the greater degradation of biomass. This was also consistent with the decrease in the yield of cellulose in the samples prepared using higher HNO_3 concentrations.

Based on the composition results, the NP25-30 and NP40-30 samples were chosen for further oxidation studies for three reasons: (i) both treated samples showed the use of 30% HNO_3 concentration can reasonably remove significant portions of lignin (66% at 25°C and 73% at 40°C) and hemicellulose (28% at 25°C and 71% at 40°C) from jute fibers, (ii) the usage of 30% HNO_3 is half of that for HNO_3 used in the one-pot NOP reaction demonstrated previously (Sharma et al., 2017), allowing for further reduction in chemicals and improvement in operational safety, and (iii) the samples with mild delignification (i.e., without intense degradation) is in fact sufficient to undergo oxidation while maintaining high mechanical strength of the scaffold.

The FTIR spectra of varying HNO_3 treated jute fibers are illustrated in Fig. 3. In these spectra, 1515 cm^{-1} peak can be assigned as the aromatic C=C stretch vibration in the lignin component, while the 1724 and 1240 cm^{-1} peaks can be assigned as the vibrations in xylan (C=O stretching) and glucomannan (C-O stretching) units, respectively, of the hemicellulose component. (Sharma et al., 2017) Similar features were observed in both sets of samples prepared at 25°C (Fig. 3(i) and 3(ii) for NP25-30) and 40°C (Fig. 3(iii) and 3(iv) for NP40-30). However, the intensities of the peaks at 1515, 1724 and 1240 cm^{-1} all decreased when the concentration of HNO_3 increased, indicating that the presence of 30% HNO_3 was effective to remove both lignin and hemicellulose components in jute fibers. In addition, the water peak at 1643 cm^{-1} corresponds to the OH bending vibration in H_2O was found to increase with increasing HNO_3 concentration (Max and Chapados, 2009), indicating that the creation of more hydrophilic cellulose after HNO_3 treatment (caused by the removal of hydrophobic lignin component the cellulose component) that has been observed previously (Eva-Lena et al., 2013; Hua et al., 2019).

The morphological changes of varying HNO_3 treated samples (NP25-15 and NP25-60, as well as NP40-15 and NP40-60) were studied by SEM,

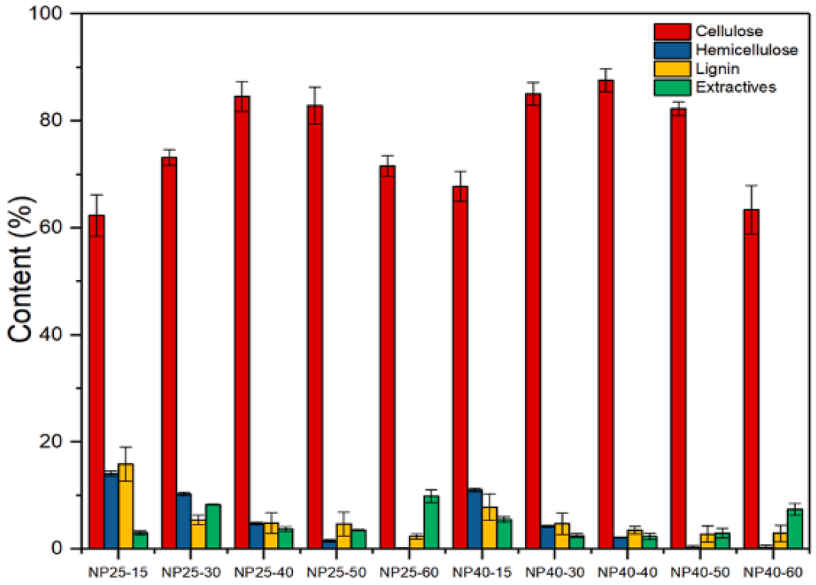

Figure 2. Summary of composition of HNO_3 treated jute fibers

where some representative images are illustrated in Fig. 4. In Fig. 4(a) and 4(b) (NP25-15), the coarse (lignin) coating on the cellulose fibers was clearly visible in, indicates that the treatment conditions: 15% HNO_3 at 25°C was too mild to induce lignin the removal in raw fibers. In contrast, the distinct fibrous texture observed in Fig. 4(c) and 4(d) (NP25-60) suggests the successful removal of the lignin component at the HNO_3 concentration (60%). The removal of the lignin component on the fiber surface exposed the underline cellulose-hemicellulose (holocellulose) fibrous network with visible pores. Similar delignification behavior was observed for HNO_3 treated jute at 40°C. In Fig. 4(e) and 4(f), the surface of the fibers was comparatively smooth with small pores, confirmed the removal of lignin even with the 15% HNO_3 treatment at 40°C. When the concentration of HNO_3 increased to 60% (Fig. 4(g) and 4(h)), the lignin component on the surface of fibers was mostly vanished, resulting in more pores on the fibers surface. These results indicate that both temperature and HNO_3 concentration can play essential roles in the removal of lignin and hemicellulose from raw lignocellulose biomass.

The crystalline structure of raw jute fiber and HNO_3 treated samples was analyzed by the WAXD technique. In Fig. 5(i) and (ii), the WAXD profiles of all treated fibers showed distinct diffraction peaks at 2θ angles of 14.9, 16.5, 22.6 and 34.5°, corresponds to $(1\bar{1}0)$, (110), (200) and (004) lattice planes of cellulose I, respectively (Chen et al., 2019; Sharma et al., 2017). These diffraction planes are characteristics of the native cellulose Iα allomorph structure produced by higher plants. However, these diffraction profiles exhibited some interesting changes with different treatment conditions. In Fig. 5(i) and 5(ii), it was seen that the peak corresponding to cellulose I $(1\bar{1}0)$ at 14.9° emerged as the concentration of HNO_3 increased (>40%). In general, the absence of $(1\bar{1}0)$ peak could be due to the presence of hemicellulose and lignin moieties around the cellulose fibers (Sharma et al., 2017). Thus, the emergence of $(1\bar{1}0)$ peak in samples (NP25-40, NP25-50, NP25-60 and NP40-40, NP40-50, NP40-60) confirmed the removal of lignin and hemicellulose. However, it was interesting to observe that in NP25-60, some diffraction peaks related to the cellulose II polymorph structure, including $(1\bar{1}0)$, (110) and (020) planes at 12.5, 20.4 and 21.9°, respectively, appeared (Sharma et al., 2014). It is known that the cellulose II structure can be formed by alkali treatment (Gupta et al., 2013) and acid treatment (Gert et al., 2003), where the cellulose molecules in the cellulose I structure are first dissolve and then recrystallize into the cellulose II structure. For example, Gupta et al. transformed cellulose I to cellulose II polymorph by using 15 wt% NaOH concentration at room temperature (Gupta et al., 2013). Gert et al. also generated the cellulose II polymorph by treating native cellulose with HNO_3 (68.5%) at room temperature, accompanied by deep decrystalization (Gert et al., 2003). In this study, we confirm that 60% HNO_3 is the critical concentration that can destroy the cellulose I structure and regenerate the cellulose II structure.

Crystallinity index (CI) and crystal size values of different HNO_3 treated samples are summarized in Table 2. A peak deconvolution method (Chi and Catchmark, 2017) was employed to deconvolute crystalline and amorphous peaks of the WAXD profiles of different HNO_3 treated samples. The results indicated that the increase in HNO_3 concentration at different range 0-50% at 25°C and 0-40% at 40°C could cause an increase in CI because of the removal of amorphous lignin and hemicellulose moieties. Compared with the CI of raw jute fiber (Figure S1 in *Supporting Information*), NP25-50 showed an increase in CI from 49.8 to 71.5%. However, a decrease in the CI value was observed in NP25-60, NP40-50, and NP40-60 samples. This indicated that higher HNO_3 concentration could further degrade the crystalline cellulose region. For example, NP25-60 showed a CI of 63% as compared to NP25-50's CI of 71%. We note that although some dissolved/degraded cellulose chains at the 60% HNO_3 condition could be recrystallized (into cellulose II polymorph), the total CI value still decreased (the peak deconvolution of the WAXD profile of NP25-60 is shown in Fig. S2 in *Supporting Information*). The cellulose I/II ratio in NP25-60 was calculated by the ratio of the area of cellulose I or that of cellulose II to the total area under the crystalline peaks. The measurements indicated that the sample prepared at 25°C with HNO_3 (60%) contains 74% of cellulose I and 26% of cellulose II. The crystal sizes of cellulose I in the directions of $(1\bar{1}0)$, (110), and (200) planes were found to increase when the HNO_3 concentration increased, further confirming the removal of lignin and hemicellulose. However, in samples NP40-50 and NP40-60, the crystal size related to the $(1\bar{1}0)$ plane in cellulose I decreased drastically. This behavior could be attributed to the dissolution of cellulose chains on the crystal surface when exposed to harsh HNO_3 treatment. Additionally, in NP25-60, the decrease in the crystal size related to the (200) plane in cellulose I and the appearance of the (020) diffraction in cellulose II further validated the recrystallization of chains into the cellulose II polymorph.

^{13}C CPMAS NMR was employed to characterize the molecular structures of treated and untreated jute fibers, where the results are shown in Fig. 5(iii) and (iv). The region between 60 and 70 ppm in the spectra could be assigned to the C6 carbon of the primary alcohol group.

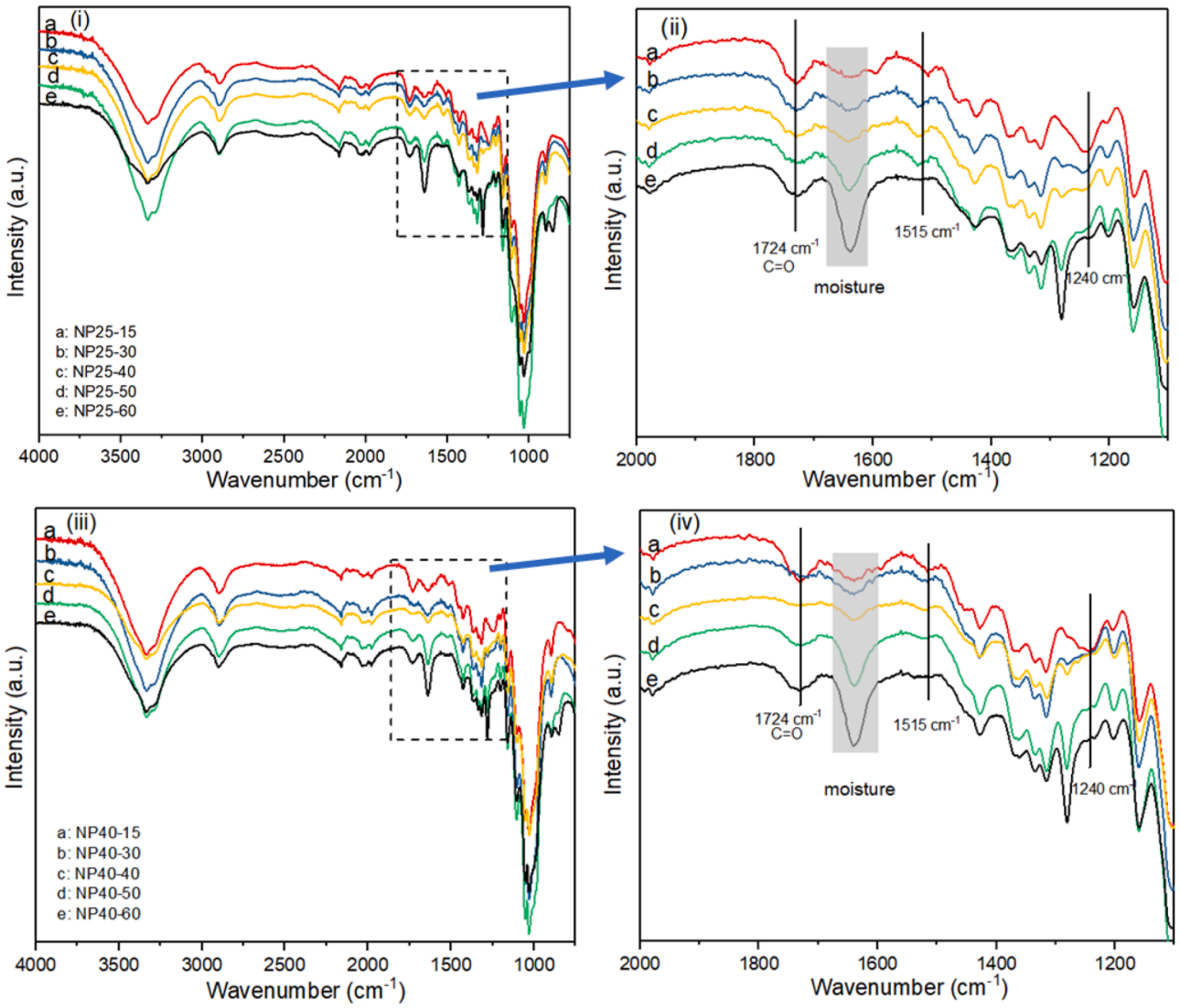

Figure 3. FTIR spectra of HNO_3 treated jute fibers with different concentrations: (i) at 25°C; (iii) at 40°C; (ii) and (iv) are enlarged versions for (i) and (iii) in the wavenumber range of 1100-2000 cm^{-1}, respectively.

The next cluster of peaks between 70 and 80 ppm could be attributed to C2, C3, and C5 carbons. The region between 80 and 95 ppm was associated with C4 carbon, and that between 100 and 110 ppm was due to the anomeric carbon C1 (Chen et al., 2019). The aromatic region around 150 ppm was assigned to the lignin unit. (Fu et al., 2015, Terrett et al., 2019). The spectra results indicated that the lignin content was significantly reduced by the HNO_3 treatment, particularly in NP25-30 and NP40-30 samples, where the aromatic region could be barely identified in the NMR spectra. The distinct peak at 175 ppm could be assigned to the carboxyl groups in hemicellulose (Garcia uriostegui et al., 2018). The spectra also showed that the hemicellulose component was reduced by HNO_3, especially in NP25-40 and NP40-30 samples.

In addition to the structure information, the solid-state NMR spectra can also provide information about the CI value from Eq. S1 (*Supporting Information*) (Park et al., 2010). The summary of CI value is also summarized in Table 2. Similar increasing trends of the CI value with increasing HNO_3 concentration were found between NMR and WAXD analyses, which confirmed that HNO_3 not only removed the lignin and hemicellulose component but probably also degraded/dissolved the amorphous region of cellulose. These results are also consistent with the quantitative chemical composition results of varying samples in Fig. 2. The CI decrease in NP25-60 could be partially attributed to the appearance of cellulose II (Gert et al., 2003). In addition, a small CHO group peak appeared at 175 ppm in NP25-60, which could be explained by the appearance of reducing end group in cellulose chain.

The thermal stability of treated samples was characterized by TGA, where the results (TGA and differential thermogravimetry (DTG) curves) are shown in Figure S3 in *Supporting Information*. The characteristic pyrolysis parameters include the onset degradation temperature (T_{onset}), maximum degradation temperature (T_{max}), weight loss, and char residues, which are summarized in Table S2 in *Supporting Information*. The first phase of decomposition in the temperature range 50–150°C could be attributed to the adsorbed moisture in the sample. The second phase of degradation around 250–370°C was assigned to the decomposition of hemicellulose, labeled as 1st degradation in Table S2. Afterward, the main degradation event occurred between 340 and 370°C could be corresponded to the degradation of α-cellulose chains by depolymerization, labeled as 2nd degradation in Table S2. The degradation of lignin occurred at a large range of temperature between 200 to 500°C. Since the degradation of hemicellulose and cellulose can lead to char formation, the accurate information regarding the decomposition of lignin is challenging by the TGA and DTG analyses. However, it was interesting to see that in Fig. S3(iii) and S3(iv), the degradation of samples with low lignin and hemicellulose contents (i.e., NP25-60,

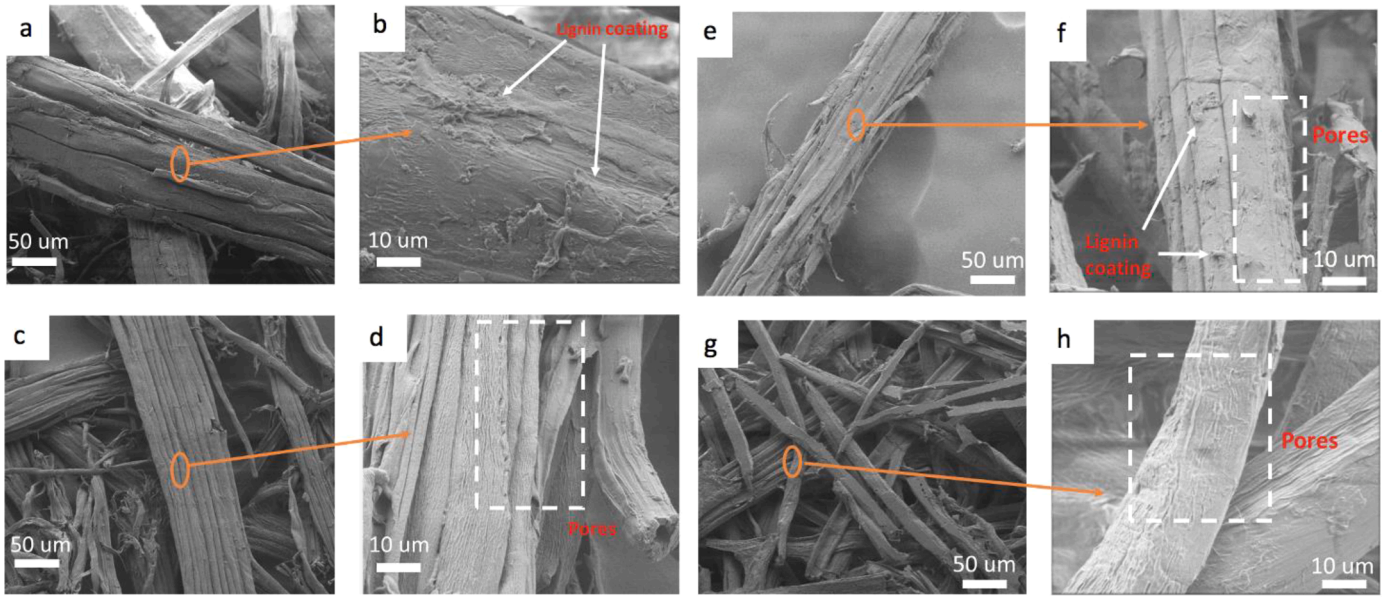

Figure 4. Representative SEM images of HNO_3 treated jute fibers: (a) NP25-15, (b) NP25-15 at higher magnification, (c) NP25-60, (d) NP25-60 at higher magnification, (e) NP40-15, (f) NP40-15 at higher magnification, (g) NP40-60, and (h) NP40-60 at higher magnification.

NP25-50, NP25-40 and NP40-60, NP40-50) started at a lower temperature. This indicated that the disappearance of the lignin component facilitated the decomposition of cellulose and hemicellulose components (Dorez et al., 2014).

3.2. *Gas-phase nitrogen dioxide (NO_2) oxidation on HNO_3 treated jute fibers*

To test the feasibility of gas-phase oxidation on HNO_3 treated samples, NP25-30 and NP40-30 were used as two model materials, where the final products after oxidation are termed as GO1 and GO2, respectively. The experimental set-up for the gaseous NO_2 oxidation treatment is shown in Fig. 1. The reaction conditions including NO_2 concentration used and the reaction temperature are summarized in Table 1. The data on the reaction yield, final COOH content, crystallinity index (CI), and crystal size for GO1 and GO2 samples are summarized in Table 3. It was found that the yield of the final products from the gas-phase oxidation using NO_2 was high (> 90%) because the gas-phase treatment avoided the hydrolysis of cellulose fibers. The initial COOH content for GO1 and GO2 was 1.63 and 1.85 mmol/g, respectively. However, after a few times washing with DI water, the COOH content stabilized at 1.31 and 1.45 mmol/g for GO1 and GO2, respectively (Fig. S4 in *Supporting Information*). This indicates that although the reaction was performed in gas-phase, it might have transformed some residual hemicellulose content, containing xylan (rich with COOH groups) into soluble products. The carboxyl contents in GO1 and GO2 were found to be higher than those reported values in NO_2 gas-phase oxidized cellulose fibers (Camy et al., 2009; Gert et al., 2005; Peng et al., 2012). For example, Camy et al. (2009) presented the oxidation of rayon cellulose using NO_2 in high-pressure CO_2 medium and achieved ~1.10 mmol/g of carboxyl content. Similarly, Gert et al. (2005) prepared carboxylated microcrystalline cellulose from bleached commercial cellulose using NO_2 and obtained 5% COOH groups with 80% yield. Notably, we used HNO_3 treated jute fibers for gas-phase oxidation instead of pure cellulose in this study. Additionally, we purged humidified N_2 into the starting samples, which allowed the moisture to wet the sample that might lead to more efficient penetration of the reactant into the fiber scaffold and facilitate the oxidation process on the cellulose surface. In the literature, this partial oxidation treatment of cellulose fibers has been termed quasi-homogeneous oxidation (Camy et al., 2009). It has been known that the presence of moisture in the reaction can play a critical role on the oxidation of cellulose.

The oxidation of GO1 and GO2 sample was confirmed by the FTIR analysis as seen in Fig. 6(i) and (ii). It was observed that the distinct peak at 1724 cm^{-1}, assigned to COOH groups, significantly increased after the NO_2 gas-phase treatment. A slight decrease in COOH peak was observed in washed samples, indicating the removal of residual hemicellulose. Additionally, the peaks at 1515 and 1240 cm^{-1} completely vanished after the gas-phase treatment, further confirmed the complete removal of lignin and hemicellulose after the treatment.

To better understand the impact of the NO_2 gas-phase treatment on the crystalline structure of cellulose fibers, WAXD profiles of GO1 and GO2 samples were also collected where the results are shown in Figure S5 (*Supporting Information*). The CI values in these samples were also calculated, where the results are shown in Table 3. It was noted that the diffraction peaks of GO1 and GO2 were almost the same as those in NP25-30 and NP25-40. Only a slight increase in the CI of samples (GO1 71.5%; GO2=78.9%) was observed as compared to NP samples. This increase might be due to the further removal of lignin and hemicellulose from NP after the NO_2 treatment. Both GO1 and GO2 samples were found to maintain the cellulose I polymorph structure, as expected.

The BET surface analysis results of GO1 and GO2 samples are presented in Fig. 6(iii) and (iv). The surface area measured for GO1 was 10.58 m^2/g, while GO2 showed a slight increase to 12.39 m^2/g. This indicates that the surface area of NO_2 treated samples was relatively higher than those of the non-oxidized cellulose fibers or liquid phase oxidized cellulose nanofibers.(surface area for non-oxidized cellulose fibers was usually in the range of 0.45-1.5 m^2/g (Bismarck et al., 2002), while for liquid phase oxidized cellulose nanofibers, surface area is around 5~7 m^2/g (Sharma et al., 2017)). The higher surface area of gas-phase treated samples were mainly due the effective oxidation process by NO_2 treatment and created more porous cellulose fibers.

3.3. *Liquid-phase (HNO_3-$NaNO_2$) oxidation on HNO_3 treated jute fibers*

The liquid-phase (HNO_3-$NaNO_2$) oxidation treatment was also conducted to compare with the gas-phase NO_2 oxidation treatment using HNO_3 treated samples. The yields for all LO samples are also summarized in Table 3. It was found that the yields of LO samples obtained by the liquid-phase treatment were relatively low (50.7- 66 %) as compared

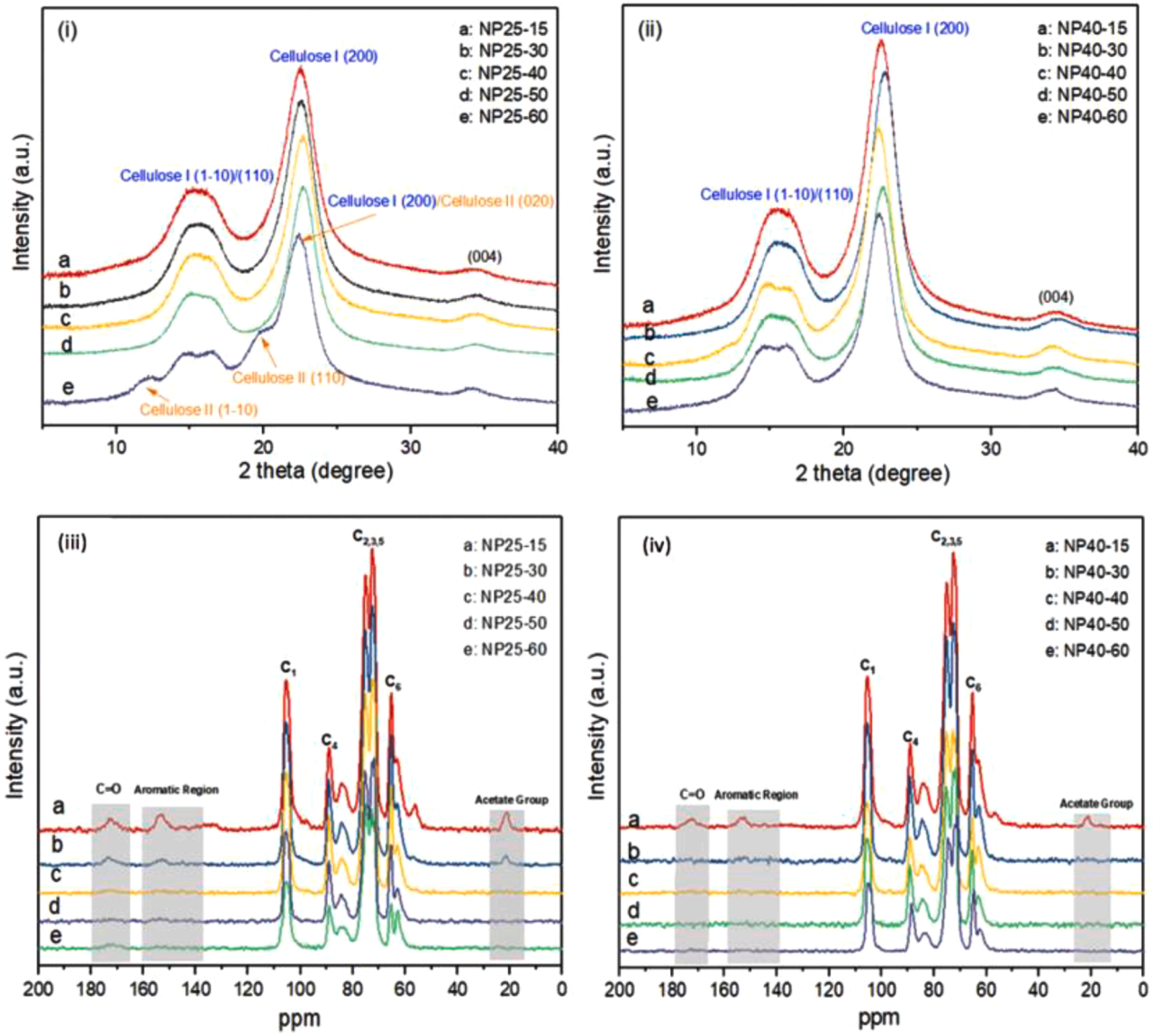

Figure 5. WAXD profiles of HNO_3 pulped samples treated at (i) 25°C, and (ii) 40°C; ^{13}C CPMAS NMR spectra of HNO_3 treated jute fibers: (iii) at 25°C; (iv) at 40°C.

Table 3
Summarized data on the yield, final COOH content, crystallinity index (CI), and crystal size for liquid-phase and gas-phase treated samples.

Samples	Yield (%)	COOH content (mmol/g)	CI (%) from WAXD	Cellulose I ($1\bar{1}0$) (nm)	Cellulose I (110) (nm)	Cellulose (200) (nm)
GO1	92.50	1.31	71.47	3.60±0	4.03 ±0.07	4.30±0
GO2	91.80	1.45	78.92	3.60±0	4.30±0.1	4.40±0
LO1	65.90	≤ 0.527	65.00	3.00±0.3	4.23 ±0.15	3.97 ±0.03
LO2	53.49		60.29	4.00±0	6.33 ±0.23	4.90 ±0.10
LO3	59.95		71.94	3.50±0	4.43 ±0.13	4.47 ±0.03
LO4	50.69		66.05	3.80±0	6.23 ±0.13	5.37 ±0.10

to those of GO sample (> 90 %). When the liquid-phase oxidation was applied to the NP40-30 samples using 60 % HNO_3 and sodium nitrite, the overall yield went down as low as 25.52% (this is because the yield for NP40-30 was 50.34% (Table 2), and the yield for LO4 was 50.69% (Table 3)). It has been reported that HNO_3 can hydrolyze the cellulose chain by cleaving the glycosidic bond, which could greatly decrease in the final product yield (Gert et al., 2006). This concern is consistent with our observation. As a result, we confirm that the gaseous NO_2 oxidation treatment seems to be a superior process over the liquid-phase oxidation treatment in terms of yield and carboxylate content. In addition, the post-treatment steps using gaseous NO_2 are simple because of less washing steps.

FTIR was conducted to qualitatively analyze the COOH groups in varying LO samples, where the spectra are illustrated in Fig. 7(i). It was found that the peak at 1724 cm^{-1}, corresponding to the COOH groups, increased with the increase of HNO_3 used in the liquid-phase oxidation treatment. The highest COOH content was observed in LO4, where 60% HNO_3 was used. The quantitative measurement of the carboxyl content in LO4 was measured using the conductometric titration, where the titration curve is shown in Fig. 7(ii). The measurement indicated that the carboxyl content in LO4 was 0.527 mmol/g, which was significantly lower than those of GO1 and GO2 obtained by the gas-phase oxidation treatment.

WAXD profiles of the liquid-phase oxidized samples are illustrated in

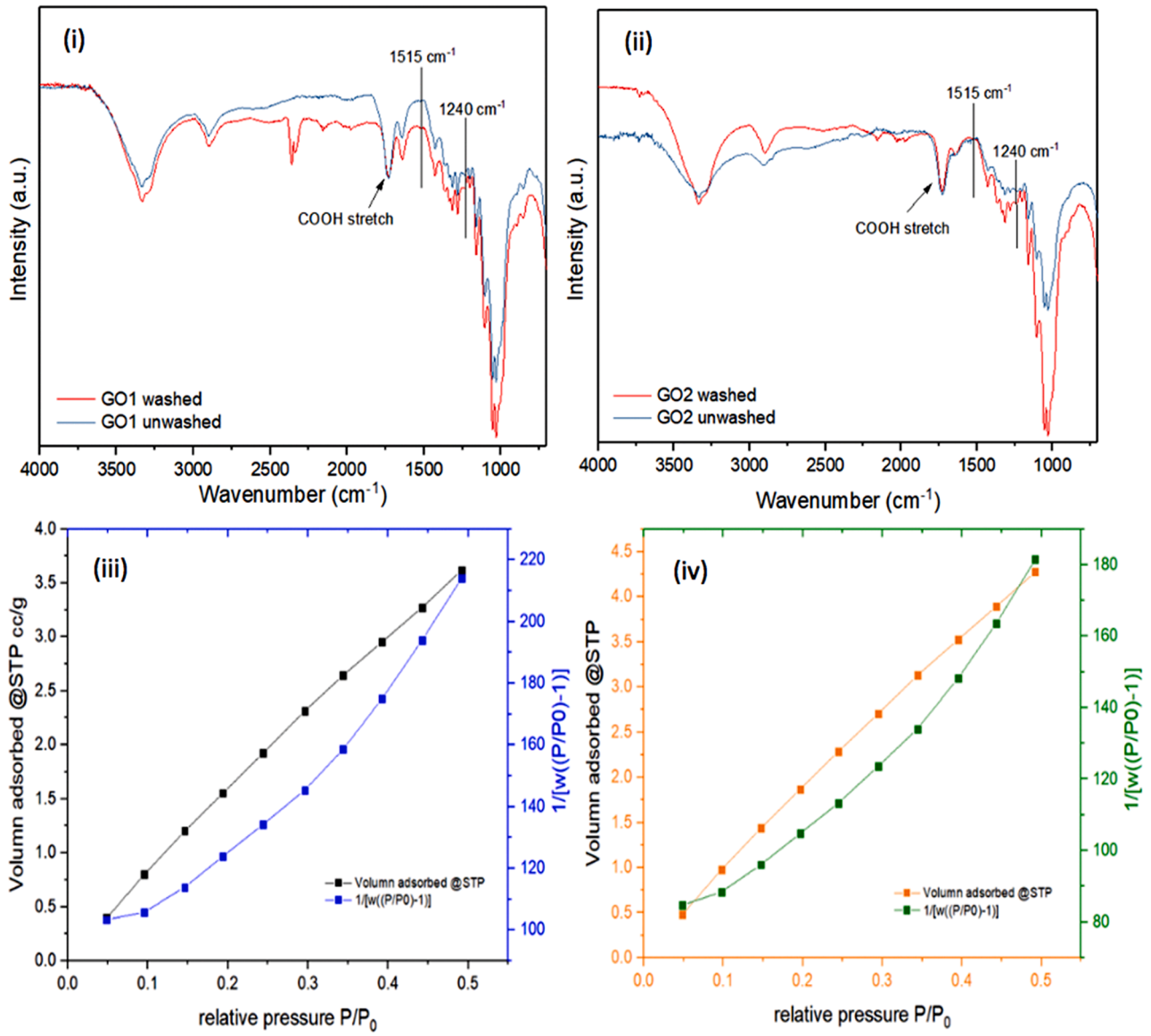

Figure 6. FTIR spectra of (i) GO1 and (ii) GO2 samples before and after washing with DI water; BET surface area analysis of gas-phase NO_2 oxidized jute fibers: (iii) GO1 and (iv) GO2.

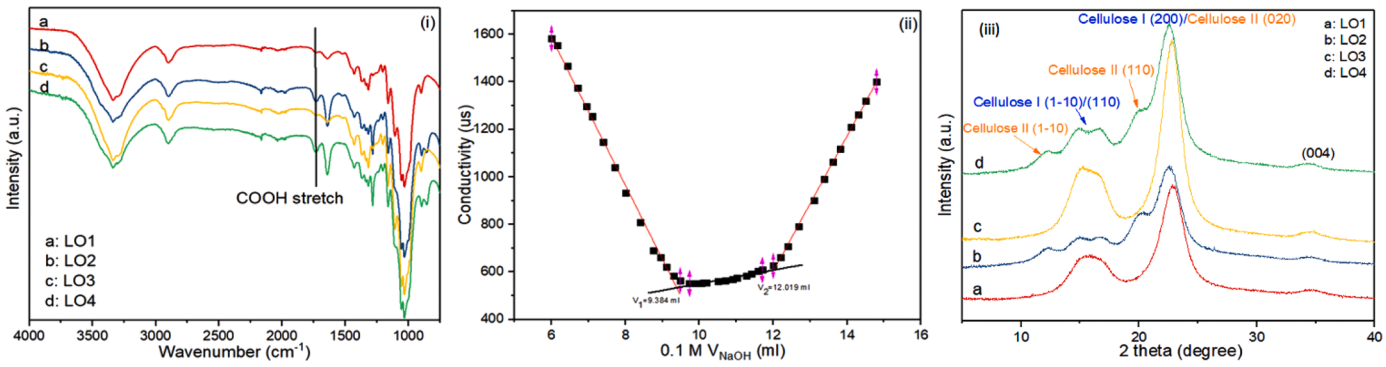

Figure 7. (i) FTIR spectra of varying liquid-phase oxidized fibers; (ii) Conductometric titration curve for LO4; (iii) WAXD profiles of liquid-phase oxidized fibers.

Fig. 7(iii). The CI values and crystal sizes of all LO samples were calculated, and the results are summarized in Table 3. It was interesting to see that with the same starting material NP25-30 (CI = 61.56%), CI became 65% for LO1, where CI became 71.47% for GO1. This implied that the liquid-phase oxidation treatment might only affect the surface of cellulose fibers, however, the gas-phase oxidation might also induce oxidation on internal cellulosic chains.

The WAXD profiles, and the corresponding peak deconvolution

analysis, for LO2 and LO4 samples are illustrated in Fig. S6 (*Supporting Information)*. It was seen that both LO2 and LO4 samples, prepared by using the 60% HNO_3-$NaNO_2$ oxidation treatment, exhibited the cellulose II structure. The deconvolution results indicated that LO2 contained 56.2% of cellulose II and 43.8 % of cellulose I, while LO4 contained 61.87 % of cellulose II and 38.13% of cellulose I. This implied that the 60% HNO_3 treatment of cellulose fibers even at room temperature can cause degradation/dissolution of cellulose chains, which would lead to the occurrence of cellulose II polymorph when recrystallized.

3.4. Thallium(I) removal by GO samples

The metal ion removal efficiency of the oxidized HNO_3-treated jute samples, prepared by post gas-phase NO_2 treatment, was evaluated using Thallium(I) as a model contaminant. Thallium(I) is one of the most toxic metal ions on the earth. The excess presence of this compound can cause lethal health effects on both humans and animals. The Thallium(I) adsorption results by GO1 and GO2 samples are shown in Tables S3 and S4, respectively (*Supporting Information*). It was seen that both GO1 and GO2 samples showed a high removal efficiency (> 80%) for a wide range of Thallium(I) concentration from 1-125 ppm. The high adsorption efficiency of GO samples was mainly due to the large content of carboxyl group on the sample surface, which caused by the electrostatic interaction between the two. Additionally, Thallium(I) removal by the LO4 sample was conducted for comparison, where the adsorption results are presented in Table S5 (*Supporting Information*). It was observed that the removal efficiency of Thallium(I) by LO4 was in the range of 59-71.6% for a wide range of TI(I) concentration from 1-125 ppm, which was significantly lower than GO samples. This can be attributed to the lower COOH content in LO4 when compared to GO samples.

Generally speaking, GO samples have shown similar removal efficiency as other best performing bioadsorbents, such as activated saw dust (92% in the presence of 50-125 ppm (Memon et al., 2008)) against the Thallium(I) removal. Therefore, we argue GO samples prepared by the liquid-gas oxidation treatment could be a low cost and promising bioadsorbent with properties similar to activated carbon to remove positively charged contaminants from water.

4. Conclusions

In this study, we demonstrated the liquid-gas phase nitro-oxidation process to prepare effective bioadsorbents directly from raw lignocellulose biomass, using jute as a model feedstock. The process involved the use of HNO_3 to delignify the biomass and the sequential gas phase (NO_2) treatment to oxidize holocellulose and generate carboxyl functional groups. It was found that the moderate 30% HNO_3 concentration was sufficient to remove a large portion of lignin and hemicellulose contents from jute fibers at room temperature. Furthermore, the NO_2 gas-phase oxidation was found to be an excellent pathway to oxidize partially delignified holocellulose cellulose. Compared to the liquid-phase (HNO_3-$NaNO_2$) oxidation treatment, gaseous NO_2 oxidation achieved higher oxidation content, greater yield, and larger crystallinity. The treatment with 60% HNO_3 at 25°C on raw jute fibers resulted in the generation of cellulose II polymorph, indicating the degradation and dissolution of cellulose chains from native crystals (cellulose I). The final product (GO1 and GO2) with efficient carboxyl content (1.31 and 1.45 mmol/g) were proven to be efficient bioadsorbents in removing a wide range of Thallium(I) concentrations from 1-125 ppm (the removal efficiency was greater than 80%). In the future, different biomass feedstocks will be tested to extend the applicability of this liquid-gas phase nitro-oxidation treatment to create low-cost and sustainable bioadsorbents with properties and performance complementary to activated carbons.

Authors statement

Hui Chen conducted the overall research and collected all the data presented. Rangjian Cao and Duning Li assisted synthesis of cellulose nanofibers. Hui Chen wrote the manuscript. Kai Chi, Sunil K Sharma, Syed M. Q. Bokhari and Ken Johnson provided guidance and helped revise the manuscript. Priyanka R. Sharma and Benjamin S. Hsiao designed the project, oversaw the progression, provided guidance and edited the manuscript.

Declaration of Competing Interest

The authors declare that they have no known competing financial interests or personal relationships that could have appeared to influence the work reported in this paper.

Acknowledgment

The financial support for this work was provided by a grant from the Polymer Program of the Division of Materials Science in the National Science Foundation (DMR-1808690) and a Partnerships for Innovation - Technology Translation (PFI-TT) grant (NSF-2140820). The authors also thank the NORAM Engineering & Construction Ltd. for assisting the NO_2 gas-phase experiments.

Supplementary materials

Supplementary material associated with this article can be found, in the online version, at doi:10.1016/j.carpta.2022.100219.

References

Abdullah, A., Rahman, C., Khan, N., & Salam, M. (1978). Preparation of microcrystalline cellulose from jute. *Bangladesh Journal of Jute and Fibre Research*.

Agarwal, A. (2007). Biofuels (alcohols and biodiesel) applications as fuels for internal combustion engines. *Progress in Energy and Combustion Science, 33*, 233–271.

Angersbach, A., Heinz, V., & Knorr, D. (2000). Effects of pulsed electric fields on cell membranes in real food systems. *Innovative Food Science & Emerging Technologies, 1*(2), 135–149.

Bajpai, P. (2018). Chapter 17 - Carbohydrate Chemistry. In P. Bajpai (Ed.), *Biermann's handbook of pulp and paper* (3rd edition, pp. 363–371). Elsevier.

Ball, P. (2005). In praise of wood. *Nature Materials, 4*(7), 515.

Bernal-Lugo, I., Jacinto-Hernandez, C., Gimeno, M., Montiel, C. C., Rivero-Cruz, F., & Velasco, O. (2019). Highly efficient single-step pretreatment to remove lignin and hemicellulose from softwood. *BioResources, 14*(2), 3567–3577.

Bismarck, A., Aranberri-Askargorta, I., Springer, J., Lampke, T., Wielage, B., Stamboulis, A., Shenderovich, I., & Limbach, H. H. (2002). Surface characterization of flax, hemp and cellulose fibers; surface properties and the water uptake behavior. *Polymer Composites, 23*(5), 872–894.

Bjerre, A. B., Olesen, A. B., Fernqvist, T., Plöger, A., & Schmidt, A. S. (1996). Pretreatment of wheat straw using combined wet oxidation and alkaline hydrolysis resulting in convertible cellulose and hemicellulose. *Biotechnology and Bioengineering, 49*(5), 568–577.

Bolker, H. I. (1965). Delignification by nitrogen compounds. Action of nitrous acid on unbleached sulfate pulp. *I&EC Product Research and Development, 4*(2), 74–79.

Brink, D. (1961). Aspects of an integrated Nitric Acid Pulping Process. *Tappi, 44*(4), 256–262.

Brink, D., Vlamis, J., & Merriman, M. (1961). Pulping process studies. II. The two-stage nitric acid: Ammonium hydroxide process and evaluation of effluents as fertilizers. *Tappi, 44*(4), 263–270.

Cadoche, L., & López, G. D. (1989). Assessment of size reduction as a preliminary step in the production of ethanol from lignocellulosic wastes. *Biological Wastes, 30*(2), 153–157.

Camy, S., Montanari, S., Rattaz, A., Vignon, M., & Condoret, J. S. (2009). Oxidation of cellulose in pressurized carbon dioxide. *The Journal of Supercritical Fluids, 51*(2), 188–196.

Chen, H., Sharma, S. K., Sharma, P. R., Chi, K., Fung, E., Aubrecht, K., Keroletswe, N., Chigome, S., & Hsiao, B. S. (2021). Nitro-oxidized carboxycellulose nanofibers from moringa plant: Effective bioadsorbent for mercury removal. *Cellulose, 28*(13), 8611–8628.

Chen, H., Sharma, S. K., Sharma, P. R., Yeh, H., Johnson, K., & Hsiao, B. S. (2019). Arsenic(III) removal by nanostructured dialdehyde cellulose–cysteine microscale and nanoscale fibers. *ACS Omega, 4*(26), 22008–22020.

Chi, K., & Catchmark, J. M. (2017). The influences of added polysaccharides on the properties of bacterial crystalline nanocellulose. *Nanoscale, 9*(39), 15144–15158.

Cosgrove, D., & Jarvis, m. (2012). Comparative structure and biomechanics of plant primary and secondary cell walls. *Frontiers in Plant Science, 3*(204).

Cox, L.; Worster, H., Assessment of some sulfur-free chemical pulping processes. Tappi Tech Ass Pulp Pap Indus 1971.

Dorez, G., Ferry, L., Sonnier, R., Taguet, A., & Lopez-Cuesta, J. M. (2014). Effect of cellulose, hemicellulose and lignin contents on pyrolysis and combustion of natural fibers. *Journal of Analytical and Applied Pyrolysis, 107*, 323–331.

Engstrom, T., & Samuelson, O. (1984). Pretreatment of kraft pulp with nitrogen dioxide and oxygen: formation of methanol. *Tappi Journal, 67*(1), 98–101.

Esteghlalian, A., Hashimoto, A. G., Fenske, J. J., & Penner, M. H. (1997). Modeling and optimization of the dilute-sulfuric-acid pretreatment of corn stover, poplar and switchgrass. *Bioresource Technology, 59*(2), 129–136.

Eva-Lena, H., Klaus, K., Janne, A., Jarmo, R., Pauli, W., Jussi, S., & Kristiina, P. L. (2013). Esterified lignin coating as water vapor and oxygen barrier for fiber-based packaging. *Holzforschung, 67*(8), 899–905.

Fatma, S., Hameed, A., Noman, M., Ahmed, T., Shahid, M., Tariq, M., Sohail, I., & Tabassum, R. (2018). Lignocellulosic biomass: A sustainable bioenergy source for the future. *Protein and Peptide Letters, 25*(2), 148–163.

Fu, L., McCallum, S. A., Miao, J., Hart, C., Tudryn, G. J., Zhang, F., & Linhardt, R. J. (2015). Rapid and accurate determination of the lignin content of lignocellulosic biomass by solid-state NMR. *Fuel, 141*, 39–45.

Galbe, M.; Zacchi, G., Pretreatment of Lignocellulosic Materials for Efficient Bioethanol Production. In Biofuels, Olsson, L., Ed. Springer Berlin Heidelberg: Berlin, Heidelberg, 2007; pp 41-65.

garcia uriostegui, L., Delgado, E., Meléndez-Ortiz, H., Camacho-Villegas, T., Esquivel, H., Gatenholm, P., & Toriz, G. (2018). Spruce xylan/HEMA-SBA15 hybrid hydrogels as a potential scaffold for fibroblast growth and attachment. *Carbohydrate Polymers, 201*.

Gert, E., Matyul'ko, A. V., Shishonok, M., Zubets, O., & Kaputskii, F. (2003). Nitric acid procedure for production of powdered cellulose II forms with various morphologies and comparison of their structural and sorption characteristics. *Russian Journal of Applied Chemistry, 76*, 1337–1343.

Gert, E. V., Torgashov, V. I., Zubets, O. V., & Kaputskii, F. N. (2005). Preparation and properties of enterosorbents based on carboxylated microcrystalline cellulose. *Cellulose, 12*(5), 517–526.

Gert, E. V., Torgashov, V. I., Zubets, O. V., & Kaputskii, F. N. (2006). Combination of oxidative and hydrolytic functions of nitric acid in production of enterosorbents based on carboxylated microcrystalline cellulose. *Russian Journal of Applied Chemistry, 79*(11), 1896–1901.

Gupta, P. K., Uniyal, V., & Naithani, S. (2013). Polymorphic transformation of cellulose I to cellulose II by alkali pretreatment and urea as an additive. *Carbohydrate Polymers, 94*(2), 843–849.

Ho, S., & Mittal, G. S. (1996). Electroporation of cell membranes: A review. *Critical Reviews in Biotechnology, 16*(4), 349–362.

Hua, Q., Liu, L.-Y., Karaaslan, M. A., & Renneckar, S. (2019). Aqueous dispersions of esterified lignin particles for hydrophobic coatings. *Frontiers in Chemistry, 7*, 515.

Itoh, H., Wada, M., Honda, Y., Kuwahara, M., & Watanabe, T. (2003). Bioorganosolve pretreatments for simultaneous saccharification and fermentation of beech wood by ethanolysis and white rot fungi. *Journal of Biotechnology, 103*(3), 273–280.

Jiménez, L., de la Torre, M. J., Maestre, F., Ferrer, J. L., & Pérez, I. (1997). Organosolv pulping of wheat straw by use of phenol. *Bioresource Technology, 60*(3), 199–205.

Kim, S., & Holtzapple, M. T. (2006). Effect of structural features on enzyme digestibility of corn stover. *Bioresource Technology, 97*(4), 583–591.

Klemm, D., Heublein, B., Fink, H. P., & Bohn, A. (2005). Cellulose: Fascinating biopolymer and sustainable raw material. *Angewandte Chemie International Edition, 44*(22), 3358–3393.

Kumar, P., Barrett, D. M., Delwiche, M. J., & Stroeve, P. (2009). Methods for pretreatment of lignocellulosic biomass for efficient hydrolysis and biofuel production. *Industrial & Engineering Chemistry Research, 48*(8), 3713–3729.

Kumar, P., Barrett, D. M., Delwiche, M. J., & Stroeve, P. (2011). Pulsed electric field pretreatment of switchgrass and wood chip species for biofuel production. *Industrial & Engineering Chemistry Research, 50*(19), 10996–11001.

Lam, H., Bigot, Y., Delmas, M., & Avignon, e. (2001). Formic acid pulping of rice straw. *Industrial Crops and Products, 14*, 65–71.

Li, Y., Zhang, X., Xiong, L., Mehmood, M., Zhao, X., & Bai, F. (2017). On-site cellulase production and efficient saccharification of corn stover employing cbh2 overexpressing Trichoderma reesei with novel induction system. *Bioresource Technology, 238*.

Lin, L., Yan, R., Jiang, W., Shen, F., Zhang, X., Zhang, Y., Deng, S., & Li, Z. (2014). Enhanced enzymatic hydrolysis of palm pressed fiber based on the three main components: Cellulose, hemicellulose, and lignin. *Applied Biochemistry and Biotechnology, 173*.

Max, J.-J., & Chapados, C. (2009). Isotope effects in liquid water by infrared spectroscopy. III. H_2O and D_2O spectra from 6000 to 0 cm− 1. *The Journal of Chemical Physics, 131*(18), Article 184505.

McDonough, T. J., The chemistry of organosolv delignification. 1992.

Memon, S. Q., Memon, N., Solangi, A. R., & Memon, J.-u.-R. (2008). Sawdust: A green and economical sorbent for thallium removal. *Chemical Engineering Journal, 140*(1), 235–240.

Moon, R. J., Martini, A., Nairn, J., Simonsen, J., & Youngblood, J. (2011). Cellulose nanomaterials review: Structure, properties and nanocomposites. *Chemical Society Reviews, 40*(7), 3941–3994.

Park, S., Baker, J. O., Himmel, M. E., Parilla, P. A., & Johnson, D. K. (2010). Cellulose crystallinity index: Measurement techniques and their impact on interpreting cellulase performance. *Biotechnology for Biofuels, 3*(1), 10.

Peng, S., Zheng, Y., Wu, J., Wu, Y., Ma, Y., Song, W., & Xi, T. (2012). Preparation and characterization of degradable oxidized bacterial cellulose reacted with nitrogen dioxide. *Polymer Bulletin, 68*(2), 415–423.

Perlack, R., Wright, L., Turhollow, A., Graham, R., Stokes, B., & Erbach, D. (2005). Biomass as feedstock for a bioenergy and bioproducts Industry: The technical feasibility of a billion-ton annual supply. *Biomass as Feedstocks for a Bioenergy and Bioproducts Industry: the Technical Feasibility of a Billion-ton Annual Supply, 72*.

Putro, J. N., Soetaredjo, F. E., Lin, S.-Y., Ju, Y.-H., & Ismadji, S. (2016). Pretreatment and conversion of lignocellulose biomass into valuable chemicals. *RSC Advances, 6*(52), 46834–46852.

Rabelo, S., Andrade, R., Filho, R., & Costa, A. (2014). Alkaline hydrogen peroxide pretreatment, enzymatic hydrolysis and fermentation of sugarcane bagasse to ethanol. *Fuel, 136*, 349–357.

Rydholm, S. A., Pulping processes. Pulping processes. 1965.

Sharma, H. K., Xu, C., & Qin, W. (2019). Biological pretreatment of lignocellulosic biomass for biofuels and bioproducts: An overview. *Waste and Biomass Valorization, 10*, 235–251.

Sharma, P. R., Chattopadhyay, A., Sharma, S. K., Geng, L., Amiralian, N., Martin, D., & Hsiao, B. S. (2018). Nanocellulose from spinifex as an effective adsorbent to remove cadmium(II) from water. *ACS Sustainable Chemistry & Engineering, 6*(3), 3279–3290.

Sharma, P. R., Chattopadhyay, A., Sharma, S. K., & Hsiao, B. S. (2017). Efficient removal of UO22+ from water using carboxycellulose nanofibers prepared by the nitro-oxidation method. *Industrial & Engineering Chemistry Research, 56*(46), 13885–13893.

Sharma, P. R., Chattopadhyay, A., Zhan, C., Sharma, S. K., Geng, L., & Hsiao, B. S. (2018). Lead removal from water using carboxycellulose nanofibers prepared by nitro-oxidation method. *Cellulose, 25*(3), 1961–1973.

Sharma, P. R., Joshi, R., Sharma, S. K., & Hsiao, B. S. (2017). A simple approach to prepare carboxycellulose nanofibers from untreated biomass. *Biomacromolecules, 18*(8), 2333–2342.

Sharma, P. R., Rajamohanan, P. R., & Varma, A. J. (2014). Supramolecular transitions in native cellulose-I during progressive oxidation reaction leading to quasi-spherical nanoparticles of 6-carboxycellulose. *Carbohydrate Polymers, 113*, 615–623.

Sharma, S. K., Sharma, P. R., Chen, H., Johnson, K., Zhan, C., Wang, R., & Hsiao, B. (2020). Cellulose-supported nanosized zinc oxide: highly efficient bionanomaterial for removal of arsenic from water (In Contaminants in our water: Identification and remediation methods). *American Chemical Society, 1352*, 253–267.

Strojny, E. J., Iwamasa, R. T., & Frevel, L. K. (1971). Oxidation of 2-methoxyethanol to methoxyacetic acid by nitric acid solutions. *Journal of the American Chemical Society, 93*(5), 1171–1178.

Sun, X. F., Sun, R. C., Tomkinson, J., & Baird, M. S. (2004). Degradation of wheat straw lignin and hemicellulosic polymers by a totally chlorine-free method. *Polymer Degradation and Stability, 83*(1), 47–57.

Terrett, O. M., Lyczakowski, J. J., Yu, L., Iuga, D., Franks, W. T., Brown, S. P., Dupree, R., & Dupree, P. (2019). Molecular architecture of softwood revealed by solid-state NMR. *Nature Communications, 10*(1), 4978.

Wichern, F., Müller, T., Joergensen, R. G., & Buerkert, A. (2004). Effects of manure quality and application forms on soil C and N turnover of a subtropical oasis soil under laboratory conditions. *Biology and Fertility of Soils, 39*(3), 165–171.

Wool, R. P. (2005). 16 - Lignin polymers and composites. In R. P. Wool, & X. S. Sun (Eds.), *Bio-based polymers and composites* (pp. 551–598). Burlington: Academic Press.

Wyman, C. E., Dale, B. E., Elander, R. T., Holtzapple, M., Ladisch, M. R., & Lee, Y. Y. (2005). Coordinated development of leading biomass pretreatment technologies. *Bioresource Technology, 96*(18), 1959–1966.

Zheng, M., Skelton, R., & Mackley, M. (2007). Biodiesel reaction screening using oscillatory flow meso reactors. *Process Safety and Environmental Protection, 85*, 365–371.